Solution Structure and Dynamics of the Small GTPase RalB in Its Active Conformation: Significance for Effector Protein Binding[†,‡]

R. Bryn Fenwick,[§,||,⊥] Sunil Prasannan,[§,||,#] Louise J. Campbell,[||] Daniel Nietlispach,[||] Katrina A. Evetts,[||] Jacques Camonis,[△] Helen R. Mott,[*,||] and Darerca Owen[*,||]

Department of Biochemistry, University of Cambridge, 80, Tennis Court Road, Cambridge CB2 1GA, U.K., and Institut Curie, Inserm U830, 26, Rue d'Ulm, 75248 Paris Cedex 05, France

Received November 18, 2008; Revised Manuscript Received January 23, 2009

ABSTRACT: The small G proteins RalA/B have a crucial function in the regulatory network that couples extracellular signals with appropriate cellular responses. RalA/B are an important component of the Ras signaling pathway and, in addition to their role in membrane trafficking, are implicated in the initiation and maintenance of tumorigenic transformation of human cells. RalA and RalB share 85% sequence identity and collaborate in supporting cancer cell proliferation but have markedly different effects. RalA is important in mediating proliferation, while depletion of RalB results in transformed cells undergoing apoptosis. Crystal structures of RalA in the free form and in complex with its effectors, Sec5 and Exo84, have been solved. Here we have determined the solution structure of free RalB bound to the GTP analogue GMPPNP to an RMSD of 0.6 Å. We show that, while the overall architecture of RalB is very similar to the crystal structure of RalA, differences exist in the switch regions, which are sensitive to the bound nucleotide. Backbone ^{15}N dynamics suggest that there are four regions of disorder in RalB: the P-loop, switch I, switch II, and the loop comprising residues 116−121, which has a single residue insertion compared to RalA. ^{31}P NMR data and the structure of RalB·GMPPNP show that the switch regions predominantly adopt state 1 (Ras nomenclature) in the unbound form, which in Ras is not competent to bind effectors. In contrast, ^{31}P NMR analysis of RalB·GTP reveals that conformations corresponding to states 1 and 2 are both sampled in solution and that addition of an effector protein only partially stabilizes state 2.

The Ras-like small G proteins, RalA/B, are important components of Ras signaling pathways, implicated in the initiation and maintenance of tumorigenic transformation of human cells, as well as vesicle transport, apoptosis, transcription, cell migration, and cell proliferation. RalA/B are bound to GDP[1] in the unstimulated state and are activated by guanine nucleotide exchange factors (GEFs). Ral GEFs are downstream of Ras (reviewed in ref *1*), and the Ral GEF pathway has been shown to be at least as important as other Ras effector pathways such as Raf and PI3-kinase in mediating aberrant growth regulation (*2, 3*). The two Ral isoforms, RalA and RalB, are 85% identical but are 100% identical over the two switch regions, which undergo conformational change upon GTP/GDP exchange in small G proteins and are usually involved in effector binding (reviewed in ref *4*). The major differences between RalA and RalB lie in the C-terminal region (the hypervariable region), between residue 180 in RalA (residue 181 in RalB) and the four C-terminal residues, which comprise the site of posttranslational geranylgeranylation required for membrane association (*5*−*7*). The differences in the hypervariable regions of RalA and RalB may be responsible for the different subcellular distribution of RalA and RalB (*8, 9*).

GTP-bound Ral binds to a number of downstream effectors, including Sec5 and Exo84, components of the octameric exocyst (or Sec6/8) complex, which mediates exocytosis by tethering vesicles to the plasma membrane (reviewed in ref *10*), RLIP-76 (Ral binding protein 1 (RalBP1) or RIP1), which is implicated in endocytosis and contains a GTPase activating domain for the Rho family G proteins, Cdc42 and Rac (*11*−*15*), the Y-box transcription factor ZONAB (ZO-1 associated nucleic acid binding protein), which regulates cell proliferation (*16*), phospholipase C-d1 (*17*), phospholipase D1 (PLD1) (*18*), and the actin filament cross-linking protein

[†] This research was supported by CR-UK Project Grant C9467/A4658 (to D.O. and H.R.M.) and Association de Recherche sur la Cancer (ARC) Grant 4845 and Agence Nationale de la Recherche (ANR) and Association Christelle Bouillot Grant ANR05BLAN033802 (to J.C.).

[‡] The atomic coordinates and structure factors (PDB code 2KE5) have been deposited in the Protein Data Bank, Research Collaboratory for Structural Bioinformatics, Rutgers University, New Brunswick, NJ (http://www.rscb.org/).

* To whom correspondence should be addressed. D.O.: tel, +44-1223-764824; fax, +44-1223-766002; e-mail, do@bioc.cam.ac.uk. H.R.M.: tel, +44-1223-764825; fax, +44-1223-766002; e-mail, hrm28@bioc.cam.ac.uk.

[§] These authors contributed equally to this work.

[||] University of Cambridge.

[⊥] Present address: Institut de Recerca Biomèdica, Parc Científic de Barcelona, c/ Baldiri Reixac 10-12, 08028 Barcelona, Spain.

[#] Present address: Division of Molecular Structure, National Institute for Medical Research (NIMR), Mill Hill, London NW7 1AA, U.K.

[△] Institut Curie, Inserm U830.

[1] Abbreviations: GDP, guanosine 5′-diphosphate; GTP, guanosine 5′-triphosphate; GMPPNP, guanylyl 5′-imidodiphosphate; GEF, guanine exchange factor; EGF, epidermal growth factor; NMR, nuclear magnetic resonance; GBD, G protein binding domain; RBD, Ral binding domain.

10.1021/bi802129d CCC: $40.75 © 2009 American Chemical Society
Published on Web 01/23/2009

filamin that acts as a scaffold linking membrane and intracellular proteins to actin (*19*).

RalA and RalB have both been implicated in tumorigenicity, but they have markedly different effects. RalA has been shown to be important in mediating proliferation, whereas RalB is implicated in mediating signals required for cell survival in cancer cells (*20*). RalA promotes anchorage-independent growth, while ectopic expression of RalB antagonizes the abilities of RalA (*21*). Depletion of RalB in these cells results in apoptosis, while, in contrast, apoptosis is relieved by depletion of RalA. For this reason RalB is a potential therapeutic target given that only cancerous cells use it to protect themselves from apoptosis (*10*). As the two Ral isoforms are so similar and indeed are identical over the switch regions, the mechanisms by which they maintain unique functions remain elusive. The molecular interactions of RalA and RalB that must underpin these functional differences are still being delineated. RalA, and not RalB, has been shown to enhance the delivery of E-cadherin to the basolateral membrane in MDCK cells, consistent with a role in regulation of the exocyst complex (*8*). In fact, the same study noted that RalB demonstrated weaker affinity for the exocyst protein Sec5 than did RalA. A distinct role for RalB, rather than RalA, in the control of cell motility has been shown, and a requirement for the exocyst in this process has also been demonstrated. Specifically, Sec5 depletion, like RalB depletion, slowed wound healing, and recruitment of exocyst components to the leading edge of motile cells was dependent on RalB rather than RalA (*22*). Finally, only RalB activates the atypical IkB kinase family member, TBK1, and this activation/recruitment is dependent on the RalB/Sec5 complex, defining a RalB effector interaction that supports the antiapoptotic properties of RalB and also implicating RalB in host defense signaling (*23*).

Small G proteins recognize their effectors through interaction with the switch regions, switch I and switch II. These are loops on the surface of the protein that couple the bound nucleotide status to recognition of binding partners. The sequences of both switches are identical in RalA and RalB. Switch II is also conserved between Ras and Ral, but the switch I sequences differ: Ras residues Ile36 and Glu37 are replaced by Lys47 and Ala48, respectively, in the Ral proteins (Figure 1). This results in an effective charge swap and is thought to be the primary reason why Ras and Ral bind different sets of effector molecules (*24*). Apart from this, the sequences of switch I in Ral and Ras are almost identical, including the conserved Thr (Thr35 in Ras, Thr46 in Ral), which is involved in the octahedral coordination of the bound Mg^{2+} ion in Ras.

In the GTP-bound or active form of small G proteins, hydrogen bonds are formed between the backbone amides of Thr35 and Gly60 (Ras) and the oxygen atoms at the γ-phosphate position, which fixes the conformation of the switch regions compared to the GDP-bound form (reviewed in ref *4*). However, several studies have revealed that Ras and other small G proteins sample two different conformations even when they are bound to GTP or its analogues (*25, 26*). These two states interconvert on a millisecond time scale and can be visualized by their characteristic ^{31}P NMR chemical shifts (*25*). State 2 is thought to be the conformation that is competent to bind effector proteins, since binding of effectors shifts the conformation equilibrium completely to this state. Furthermore, certain mutations can shift the equilibrium in favor of one of the states. The molecular basis for these two states has been postulated to be the proximity of switch I to the nucleotide phosphate groups. In state 2, switch I is thought to be closer to the phosphates, which are then subjected to a ring current shift from Tyr32 (Ras numbering), whereas in state 1, the side chain of Tyr32 is oriented away from the nucleotide. This is supported by X-ray derived structures of Ras with GTP analogues and that of the closely related GTPase Rap1a in complex with the Ras binding domain of Raf-1. The change in the side chain position of Tyr32 is part of a concerted change in the dynamics of three regions of Ras: switches I and II and the P loop (*25, 26*).

Several crystal structures of RalA have been published. The free structure has been solved in complex both with GDP (*24, 27*) and with the GTP analogue, GMPPNP (*27*). Structures of RalA·GMPPNP in complex with the exocyst subunits Sec5 (*28*) and Exo84 (*29*) have also been elucidated. Sec5 binds predominantly to switch I of RalA, while Exo84 binds to both switches. The complex of RalA·GDP bound to the *Clostridium botulinum* exoenzyme C3 (C3bot) was also recently solved (*30, 31*).

Here, we present the first structure of free RalB, bound to the GTP analogue GMPPNP. We have analyzed the backbone amide dynamics of the protein, and this, along with the structure, suggests that the switch regions of RalB·GMPPNP, like those of many G proteins, are relatively mobile. ^{31}P NMR data show, however, that RalB·GMPPNP preferentially samples state 1, which in Ras is the inactive conformation, in solution but that addition of the effector Sec5 leads to a switch to the state 2 conformation. In contrast, RalB·GTP samples both conformations in solution, and addition of excess Sec5 does not force a complete switch to the (presumably) active, state 2 conformation.

EXPERIMENTAL PROCEDURES

Protein Expression and Purification. Human RalA (residues 1−192) and RalB (residues 1−185), containing the activating mutation Q72L (henceforth referred to as RalA or RalB), were cloned into pET16b (Novagen), using *Nde*I and *Bam*HI restriction sites. The Q72L mutation has been used extensively in structural studies to decrease the GTP hydrolysis activity of small G proteins and to stabilize the active form of the proteins (*29, 32, 33*). T46A and T46S mutations were introduced into the RalB expression construct using the QuikChange multi-site-directed mutagenesis kit (Stratagene). The sequences of the RalB coding regions of the mutants were verified using an automated DNA sequencer (Applied Biosystems Inc.) by the DNA Sequencing Facility, Department of Biochemistry, University of Cambridge. All Ral proteins were expressed in *Escherichia coli* strain BL21(DE3) (Invitrogen). Uniformly ^{15}N and ^{15}N,^{13}C-labeled RalB was produced as described previously (*34*). The protein was concentrated to ~0.6 mM and the bound nucleotide exchanged for the nonhydrolyzable analogue GMPPNP or GTP (Sigma) as described previously (*35*). Presence of the bound nucleotide was confirmed by HPLC analysis. His-tagged murine Sec5 (residues 5−97) for ^{31}P NMR studies was expressed and purified from a pET16b

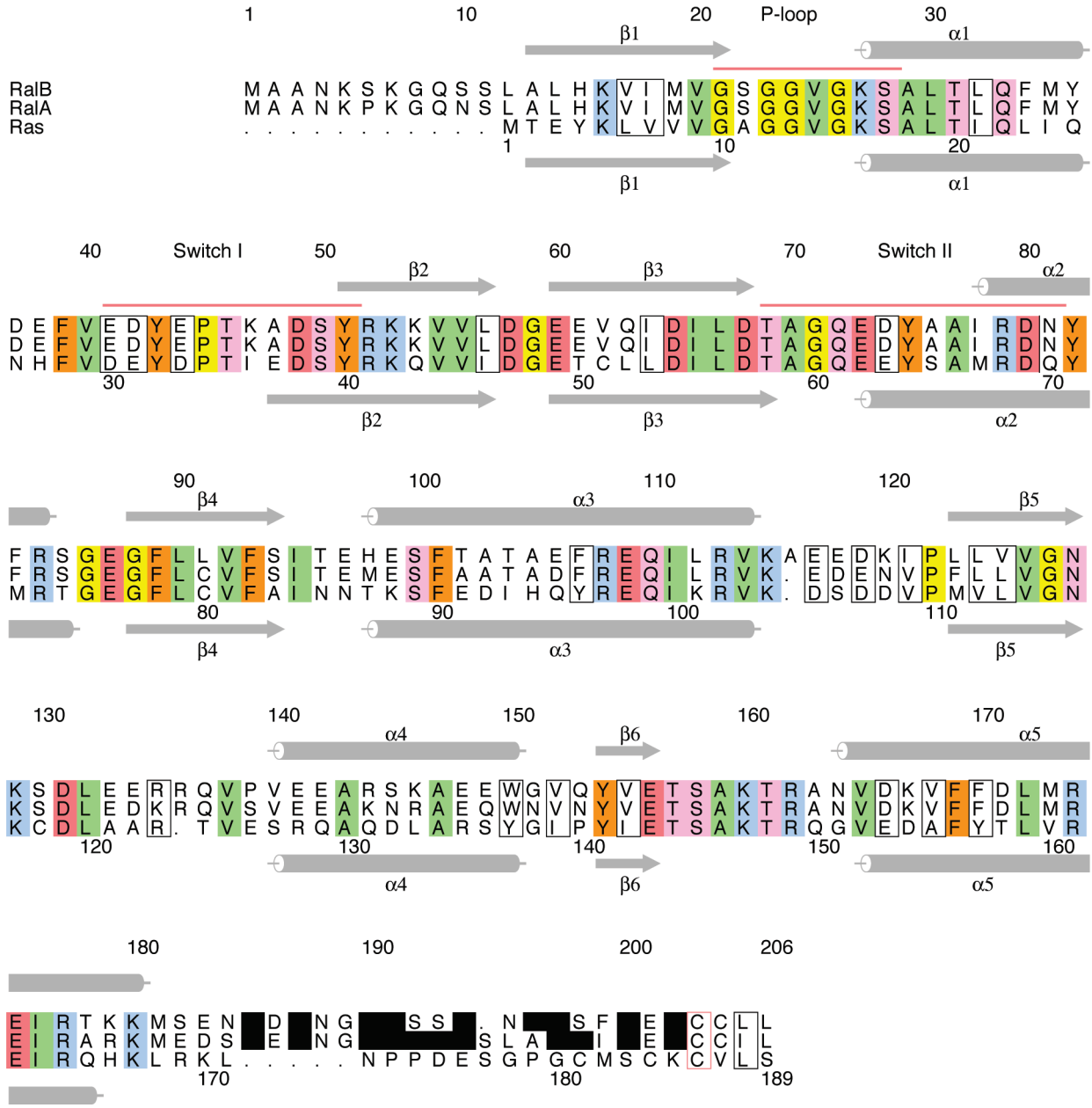

FIGURE 1: Sequence alignment of RalB (top), RalA (middle), and Ha-Ras (bottom) with secondary structure elements for Ha-Ras below and RalB above. Red bars indicate the P-loop and switch I and switch II regions. The conserved residues are shaded: Gly/Pro (yellow), Ser/Thr/Gln/Asn (magenta), hydrophobic aliphatic (green), aromatic (orange), acidic (red), and basic (blue). Open boxes indicate conservative substitutions. Black boxes indicate basic residues in the C-terminal hypervariable domain of RalA and RalB. The conserved Cys residue in the CAAX box is boxed in red.

construct as previously described (*36*). Murine Sec5 (residues 5−97) for SPA studies was expressed as a GST fusion from the vector pGEX-2T, cloned using *Bam*HI and *Eco*RI restriction sites (GE Healthcare). GST-Sec5 was expressed in *E. coli* BL21 (Novagen). Stationary cultures were diluted 1 in 10, grown at 37 °C to an OD_{600} of 0.8, and induced with 0.1 mM IPTG for 5 h. Proteins were then affinity purified using glutathione−agarose beads (Sigma-Aldrich) and eluted with 10 mM glutathione (Sigma-Aldrich). The protein was finally purified by gel filtration (S75 16/60; GE Healthcare).

[^{3}H]GTP Nucleotide Exchange. [8,5′-^{3}H]GTP (GE Healthcare; 0.15 mCi) was dried by centrifugal evaporation. To this was added RalB protein (0.7 mg in a volume of 0.14 mL), followed by 0.5 μL of 1 M KCl and 15 μL of 3 M $NH_4(SO_4)_2$ making a final volume of 155.5 μL. The mixture was incubated at 37 °C for 2 h, and then 1 μL of 1 M $MgCl_2$ was added. Unbound nucleotide was removed using a 1 mL Sephadex G25 (superfine; GE Healthcare) centrifuge gel filtration column in 10 mM Tris-HCl, pH 7.5, 100 mM NaCl, 1 mM $MgCl_2$, and 1 mM dithiothreitol.

Scintillation Proximity Assays. Affinities of RalA, RalB, RalB T46A, and RalB T46S for GST-Sec5 were measured using scintillation proximity assays (SPAs), in which GST fusion protein was attached to a fluoromicrosphere via an anti-GST antibody in the presence of Q72L RalA·[^{3}H]GTP, Q72L RalB·[^{3}H]GTP, Q72L T46A RalB·[^{3}H]GTP, or Q72L T46S RalB·[^{3}H]GTP in assays used analogous to those used with other effectors and GAPs (*37*−*41*). Binding of the G protein to the GST-Sec5 brings the labeled nucleotide close enough to the scintillant to obtain a signal. Apparent K_ds were measured as described previously (*35*) by varying the

concentration of RalA/B·[^{3}H]GTP at a constant concentration of GST-Sec5. These assays were performed with 20 nM GST-Sec5. Using this method, the upper and lower limits of the K_ds that can accurately measured are 1000 and 1 nM, respectively. For each affinity determination, data points were obtained for at least ten different RalA/B concentrations. Binding curves were fitted using the appropriate binding isotherms to obtain K_d values and their standard errors (*35, 42*).

NMR Spectroscopy. NMR samples used for structure determination and dynamics comprised ~0.6 mM protein in 50 mM sodium phosphate, pH 7.6, 100 mM NaCl, 1 mM $MgCl_2$, and 0.05% NaN_3 (NMR buffer) to which was added 10% D_2O. The unlabeled samples used for ^{31}P NMR comprised ~0.4 mM RalB·GMPPNP or ~0.6 mM RalB·GTP in 10 mM Tris-HCl, pH 7.4, 200 mM NaCl, 1 mM $MgCl_2$, 0.05% NaN_3 or 0.6 mM RalB, and 1.2 mM GTPase binding domain (GBD) of Sec5 in the same buffer. The concentrations of RalB and Sec5 were determined by amino acid analysis (Protein and Nucleic Acid Chemistry Facility, Department of Biochemistry, University of Cambridge). Experiments were recorded on a Bruker DRX500 except for the ^{13}C HSQC and ^{13}C-separated NOESY, which were recorded on a Bruker DRX800. All experiments were recorded at 25 °C unless stated otherwise. The following experiments were recorded on ^{15}N,^{13}C-labeled RalB: HNCA, HN(CO)CA, HNCACB, CBCA(CO)NH, HBHA(CBCACO)NH, HNCO, (H)C(CCO)NH, HCCH-TOCSY, and 3D ^{13}C-separated NOESY. A 3D ^{15}N-separated TOSCY and ^{15}N-separated NOESY were recorded on a ^{15}N-labeled sample. A 2D homonuclear ^{1}H NOESY was recorded on unlabeled RalB. All NOESY mixing times were 100 ms. NMR data were processed using AZARA (W. Boucher, Department of Biochemistry, University of Cambridge, unpublished) and analyzed using CCPN Analysis (*43*). The resonances were assigned as previously described (*34*). Distance restraints were generated by analyzing ^{15}N-separated and ^{13}C-separated NOESY spectra. The 2D homonuclear NOESY was used to identify proton chemical shifts for the bound GMPPNP. For ^{31}P NMR, spectra were recorded at 25 and −6 °C, at 202 MHz (corresponding to a 500 MHz proton frequency).

Backbone Dynamics. 2D ^{1}H−^{15}N correlation spectra (*44*) were recorded on ^{15}N-labeled RalB·GMPPNP to determine ^{15}N relaxation times and the ^{1}H−^{15}N NOE. The ^{15}N T_1 and T_2 series of spectra were recorded as pseudo-3D experiments. T_1 experiments were recorded with time delays of 0.01, 0.05, 0.10, 0.15, 0.25, 0.40, 0.50, 0.60, 0.70, and 0.80 s, and the T_2 series were recorded with delays of 0.0144, 0.0288, 0.0432, 0.0576, 0.0720, 0.0864, 0.1008, and 0.1152 s. The relaxation data were analyzed using CCPN Analysis (*43*), fitting a relaxation time and associated error for each residue (*45*). T_1 and T_2 decays were fitted to an exponential: $I(t) = I_0 \exp(-t/T_{1,2})$. Steady-state NOE data comprised a single pair of reference and saturated experiments. The peak heights were measured, and the intensity ratios (I_{sat}/I_{ref}) were calculated. The error in the NOE, d(NOE), was estimated as

$$\delta(\mathrm{NOE}) = \mathrm{NOE}\sqrt{\left(\frac{\delta I_{sat}}{I_{sat}}\right)^2 + \left(\frac{\delta I_{ref}}{I_{ref}}\right)^2}$$

where δI_{sat} and δI_{ref} are the noise levels in the saturated and reference experiments, respectively.

The relaxation data were analyzed using the program Tensor2 (*46*), based on the residue-specific R_1 and R_2 relaxation rates, the heteronuclear NOE values, and the coordinates of RalB·GMPPNP structure closest to the mean. The average R_2/R_1 was calculated using relaxation data for those residues in secondary structure that were deemed not to have significant internal motion, i.e., those with heteronuclear NOE values more than 0.65. The expression

$$\theta = \frac{\langle T_2 \rangle - T_{2n}}{\langle T_2 \rangle} - \frac{\langle T_{1n} \rangle - \langle T_1 \rangle}{\langle T_1 \rangle}$$

was evaluated to determine which T_1/T_2 ratios were affected by motional anisotropy (*47, 48*, J. Kirkpatrick, personal communication), where $\langle T_x \rangle$ is the average T_1/T_2 and T_{xn} is the T_1/T_2 of that residue. Residues whose value for θ were significantly larger than 0 (i.e., more than 1.5 times the standard deviation of all values of θ) were assumed to be experiencing exchange broadening and were not included in the average R_2/R_1. The average R_2/R_1 was calculated for residues 15−20, 28, 30−33, 36, 51−57, 60−67, 78, 80−82, 88, 91−93, 103−104, 106−107, 109−115, 125−128, 130−135, 140, 142−149, 155, 164−173, and 175−181 and was used to obtain an estimate for the overall correlation time, τ_c. Order parameters (S^2) were calculated for all residues for which data were available, using the calculated τ_c value obtained above and an N−H bond length of 1.02 Å. Data were analyzed using the Lipari−Szabo model-free formalism (*49, 50*) or the extended model (*51*), assuming anisotropic tumbling of the protein. The data were fitted to one of five models: model 1, S^2 only; model 2, S^2, τ_I (correlation time for internal motion); model 3, S^2, R_{ex} (chemical exchange contribution); model 4, S^2, τ_i, R_{ex}; model 5, extended model, including a very fast and a slower internal motion characterized by two order parameters (S_f^2 and S_s^2) and two internal correlation times, one of which, τ_f, is assumed to be close to 0 and τ_s (where $\tau_f < \tau_s < \tau_c$). In each case, the F-statistic was used to justify the inclusion of extra parameters (*52*).

Structure Calculation. CCPN Analysis (*43*) was used to generate unambiguous and ambiguous restraints from the ^{13}C-separated NOESY, ^{15}N-separated NOESY, and 2D homonuclear NOESY spectra. Tolerances for chemical shift matching were set to ±0.05 ppm in the direct ^{1}H dimension, ±0.07 ppm in the indirect ^{1}H dimension, ±0.30 ppm for ^{13}C, and ±0.40 ppm for ^{15}N. The backbone dihedral angles, ϕ and ψ, were estimated from the C^α, C^β, C', H^N, N, and H^α chemical shifts using the program TALOS (*53*). For those residues whose ϕ and ψ could be predicted by TALOS, backbone dihedral restraints were used, with errors set to twice the standard deviation of the TALOS prediction. The GMPPNP nucleotide was modeled in by adding restraints to coordinate the Mg^{2+} ion to two water molecules, the $O^{2\beta}$ and $O^{2\gamma}$, and the side chain oxygen atom of Ser28 in RalB, as we have used previously in other G protein structures (*32*). Also included were conserved H-bonds between the backbone nitrogen atom of Gly71 and GMPPNP$^\gamma$ $O^{3\gamma}$.

Structures were calculated using ARIA 1.2 (*54*) and CNS 1.1 (*55*), where the ambiguity of the restraints was decreased by calculating 20 structures in eight iterations (*54*). In the final iteration, 100 structures were calculated, and the 40 with the lowest energy were refined in explicit water and selected for further analysis.

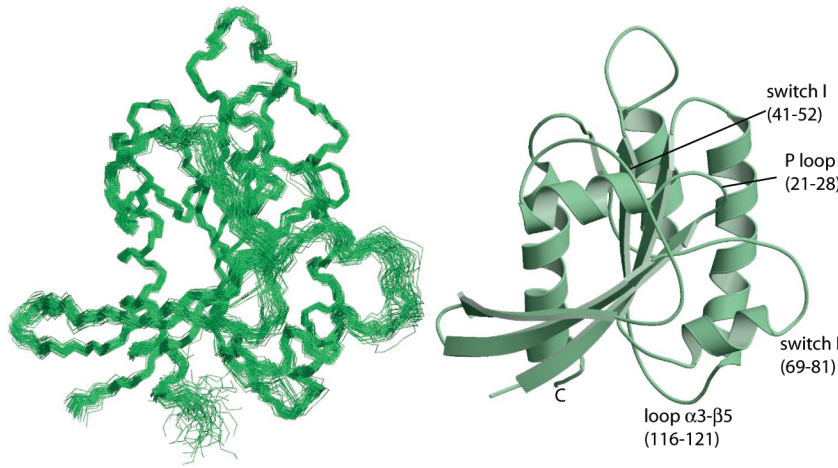

FIGURE 2: Family of 40 lowest energy RalB·GMPPNP NMR structures (left) and the closest to the mean structure (right). This figure was made using Molscript (*70*) and Raster3D (*71*). PDB code 2KE5.

RESULTS

Resonance Assignment. The backbone resonances were assigned using standard 3D triple resonance NMR approaches (reviewed in ref *56*). Backbone amide resonances were not observed for some residues in the switch regions: 44, 47, 48, 69, 70, and 74 (Figure 1). A similar phenomenon has been observed in NMR studies of other small GTPases, such as Ras (*26*) and Cdc42 (*57*), where it was found that while a full or near-complete backbone assignment could be made for the GDP-bound protein, resonances in the switches in the active form were attenuated. No backbone amide resonances were visible for residues 1−11, and subsequent N-terminal sequencing showed that the N-terminus in the NMR sample had been proteolytically cleaved. This region is outside the G domain and unlikely to be structured.

Side chains were assigned for all residues in RalB·GMPPNP for which backbone resonances could be observed, except Glu73. Side chains were also assigned for several residues in the switch regions whose amides were not observed: residues 44, 48, 69, 70, and 74. Chemical shift assignments have been deposited in the BMRB database with accession number 15230 (*34*).

The H1, H2, and H8 shifts for the purine ring and H1′ in the ribose ring in GMPPNP were assigned from the 2D ^{1}H NOESY spectrum, using the random coil nucleotide shifts (*58*), and had ^{1}H chemical shifts of 13.06, 6.36, 7.94, and 6.02 ppm, respectively.

Structure Calculation. ϕ and ψ restraints (110 pairs) were predicted from the chemical shifts using TALOS (*53*). A total of 5021 NOEs were translated by ARIA into 4709 unique restraints, of which 2619 were unambiguous and 2090 were ambiguous. At the end of the final iteration, there were 4552 unique NOEs, comprising 3456 unambiguous and 1096 ambiguous restraints. The final structure had no NOE violations more than 0.5 Å and no dihedral angle violations more than 5°.

Solution Structure of RalB·GMPPNP. The structure of RalB·GMPPNP is well defined by the data and of good quality, with an overall backbone RMSD of 0.60 ± 0.09 Å (Figure 2, Table 1, PDB code 2KE5). The structure is a classical small GTPase domain (reviewed in ref *4*), comprising a six-stranded β-sheet (β1−6) surrounded by five α-helices (α1−5) (Figures 1 and 2). The six β-strands encompass residues 13−21, 51−57, 60−68, 88−94, 123−128, and 154−156 and the five canonical α-helices encompass residues 27−36, 78−84, 98−114, 140−150, and 164−180. Switch I extends over the first residue of strand β2, while switch II incorporates the first four residues of helix α2. The backbone RMSD across the family for switch I (residues 41−51) was 0.63 ± 0.20 Å, while for switch II (69−81) it was 0.85 ± 0.21 Å.

Backbone Amide Dynamics. Experimental relaxation data consisting of ^{15}N longitudinal relaxation times (T_1), transverse relaxation times (T_2), and the steady-state ^{1}H−^{15}N NOE were obtained for all residues whose backbone amide resonances were assigned, unless they were overlapped in the ^{15}N HSQC spectra. Relaxation parameters were thus available for a total of 139 residues. Plots of T_1, T_2, and the NOE are shown in Figure 3. The average and standard deviations for T_1, T_2, and the NOE are 729.96 ± 58.32 ms, 71.73 ± 6.77 ms, and 0.78 ± 0.10, respectively. Residues that were not affected by internal motion were used to estimate an overall correlation time for isotropic tumbling of 11.75 ns using Tensor2 (*46*). The relaxation data for RalB, however, are consistent with its approximate behavior in solution as a prolate ellipsoid, with principal components of the rotational diffusion tensor of 1.319×10^7 s^{-1}, 1.379×10^7 s^{-1}, and 1.616×10^7 s^{-1}. Experimental data for all 139 residues for which measurements were available were utilized to calculate order parameters (S^2) assuming anisotropic rotational diffusion as well as corrections for chemical exchange (R_{ex}) and effective correlation times for fast internal motions (τ_e), where applicable (Figure 4). Corrections for chemical exchange were necessary for residues at the N- and C-termini (Ala13 and Thr178), Phe83 at the C-terminus of switch II, and Lys129 and Val138, which are at either end of a long loop between strand β5 and helix α4.

The relaxation data show that there are four major regions of mobility in RalB outside of the extreme termini. Residues in the P-loop, 21−28, which forms part of the nucleotide binding site are experiencing motion on a range of time scales. Gly21 has a short T_1 and low heteronuclear NOE value and was modeled with an internal correlation time of ~1.5 ns, whereas Ser22 and Ser28 have short T_2s and high heteronuclear NOE values, suggesting that they are moving

Table 1: Structural Statistics for RalB·GMPPNP

		⟨SA⟩[a]	⟨SA⟩$_c$[b]
Experimental Restraints Used in Structure Calculation			
unambiguous NOEs	3473		
ambiguous NOEs	1092		
dihedral angle restraints ($\phi + \psi$)	256		
Structural Statistics			
Coordinate Precision (Å)			
RMSD of backbone atoms (13−183)		0.60 ± 0.08	0.46
RMSD of heavy atoms (13−183)		1.07 ± 0.11	0.98
RMSD of backbone atoms (13−40, 52−68, 83−183)		0.47 ± 0.07	0.40
RMSD of backbone atoms (41−51)		0.63 ± 0.20	0.59
RMSD of backbone atoms (69−82)		0.84 ± 0.20	0.69
RMSD from Experimental Restraints			
NOEs distances (Å)		$9.54 \times 10^{-3} \pm 6.84 \times 10^{-4}$	1.09×10^{-2}
dihedral angles (deg)		$(0.45 \pm 3.86) \times 10^{-2}$	0.44
RMSD from Idealized Geometry			
bonds (Å)		$1.38 \times 10^{-3} \pm 4.41 \times 10^{-5}$	1.40×10^{-3}
angles (deg)		$(0.32 \pm 4.04) \times 10^{-3}$	0.31
impropers (deg)		$(0.22 \pm 6.70) \times 10^{-3}$	0.22
Final Energy (kJ/mol)			
$E_{L\text{-}J}$[c]		−1693.7 ± 12.39	−1699.61
Ramachandran Analysis[d]			
most favored regions (%)		86.0	86.2
allowed regions (%)		11.9	13.2
generously allowed regions (%)		1.5	0.6
disallowed regions (%)		0.6	0.0

[a] ⟨SA⟩ represents the average RMS deviations for the ensemble. [b] ⟨SA⟩$_c$ represents values for the structure that is closest to the mean. [c] The Lennard-Jones potential was not used at any stage in the refinement. [d] PROCHECK (*69*).

on a millisecond time scale. Val25, also in the P-loop, was modeled using two order parameters and an internal correlation time >10 ns.

As described above, several backbone resonances for residues in switch I (41−51) were absent from the ^{15}N HSQC spectra, presumably due to chemical exchange. Many of the remaining resonances in this region were weak or overlapped, preventing accurate measurement of their intensities. Although this precludes a quantitative analysis of the dynamics of this region, it suggests that most of the residues in switch I are undergoing slow motion on the ^{15}N time scale. Residues Glu41 and Asp42 at the N-terminus of switch I have low heteronuclear NOE and T_1 values and so are involved in motion on the picosecond to nanosecond time scale, and indeed Glu41 was modeled with an internal correlation time of ∼1.2 ns. At the other end of the switch, Tyr51 is relatively rigid, since it has an order parameter of 0.98 and no evidence of motion from the T_1, T_2, or NOE values.

Similarly, two residues in switch II (69−81) were missing resonances in the ^{15}N HSQC, and several other resonances in this region were too overlapped for quantitative analysis. For those residues that could be analyzed, Ala77 has a low heteronuclear NOE and Asp80 a low T_1 value, suggesting that these residues are both involved in dynamics on a picosecond time scale. These residues are on the exterior surface of the switch II α-helix. Other residues in the helix have slightly lower order parameters, and there is more evidence for dynamics at the C-terminus of the helix, where Phe83 has a low T_2, indicating millisecond time scale motion while Ser85 has a low heteronuclear NOE and was modeled with an internal correlation time of ∼1.2 ns.

Interestingly, the only loop of RalB that displays concerted motion is the region between 116−121. Within this loop every residue has a lower order parameter than average (Figure 4); all residues were modeled using an internal correlation time, and all but one had to be modeled using the extended Lipari−Szabo model (*51*), i.e., with internal motion on fast and slow time scales. Comparison of the sequences of RalA and RalB (Figure 1) reveals that this region is the site of a single amino acid insertion in RalB, Ala116.

^{31}P NMR. To investigate further the dynamics of the switch regions, particularly switch I, we recorded ^{31}P NMR experiments to investigate the chemical environment of the nucleotide. The ^{31}P NMR spectrum of RalB·GMPPNP at 25 °C contained, as expected, three resonances, corresponding to the three phosphate groups in the GMPPNP (Figure 5a) as well as a resonance from residual phosphate in the sample. The chemical shifts of the three resonances were 1.04, −2.33, and −10.11 ppm and could be assigned to the β-, γ-, and α-phosphates, respectively, based on the published chemical shifts of GMPPNP in complex with Ha-Ras (*59*). In several other G proteins, such as Ha-Ras (*25*), two species are observed at lower temperatures (around 5 °C) for one or two of the ^{31}P resonances. State 1, which is shifted downfield, is thought to be in a conformation that is not competent to bind effector proteins, whereas the upfield-shifted component, state 2, is thought to be the active conformation. To determine whether RalB·GMPPNP also samples these two states, the ^{31}P NMR spectra were recorded at lower temperatures. Even at −6 °C, although the resonances were significantly broadened, no splitting of the peaks was observed (Table 2, Figure 5b).

It is not possible to determine whether the single resonance observed for RalB corresponds to a bias in the population toward state 1 or state 2 or is due to fast exchange between the two states. To allow us to distinguish between these possibilities, we reasoned that adding an effector should stabilize the active, state 2, conformation of the G protein. This would therefore allow the chemical shifts of the

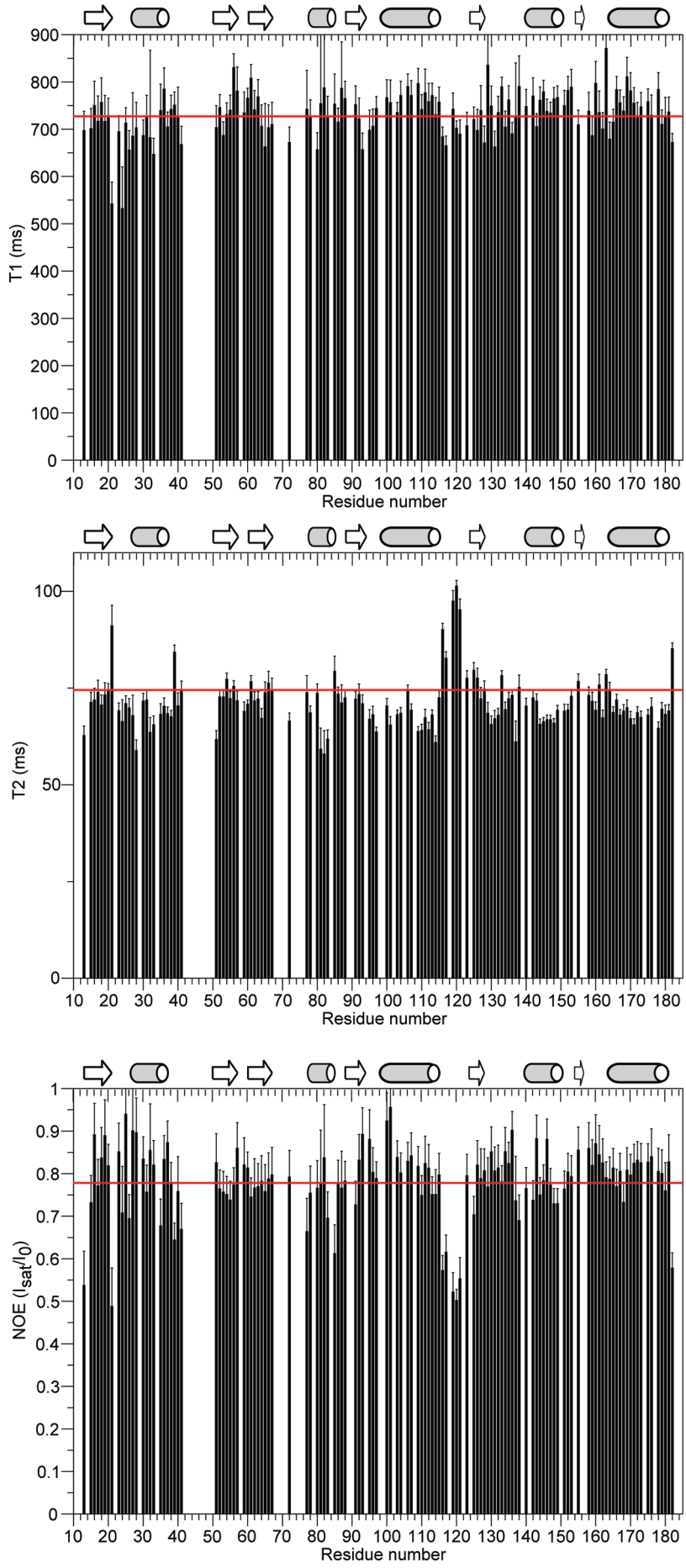

FIGURE 3: ^{15}N T_1, T_2, and heteronuclear NOE values for the backbone amides of RalB·GMPPNP. Data were excluded for overlapped peaks. Mean values are indicated by the red lines.

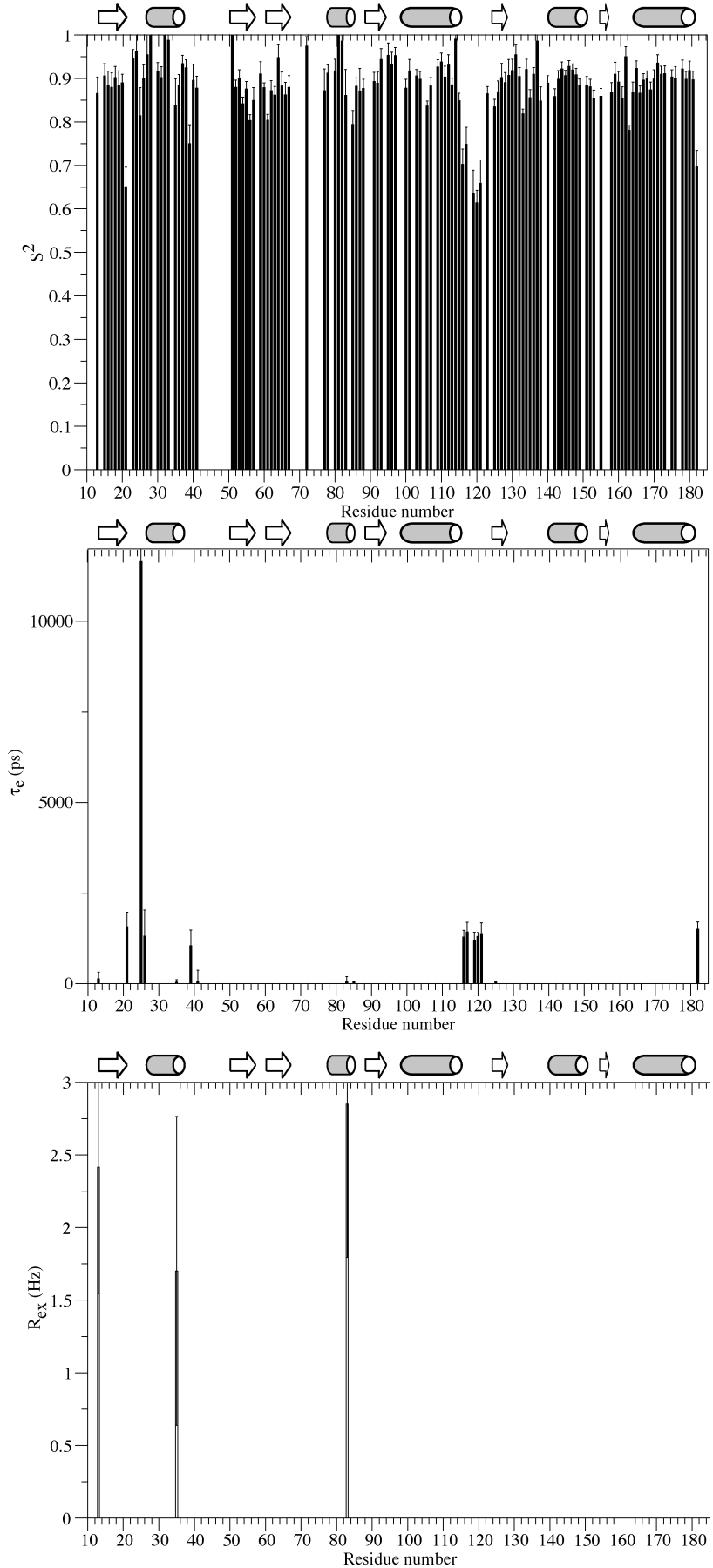

FIGURE 4: Backbone dynamic parameters for RalB·GMPPNP calculated from a model-free analysis, assuming that the overall motion is anisotropic: S^2 (order parameter) in the top panel (for residues 116−121, 164, and 182, $S^2 = S^2_f S^2_s$), τ_e (effective internal correlation time) in the middle panel, and R_{ex} (exchange contribution) in the bottom panel.

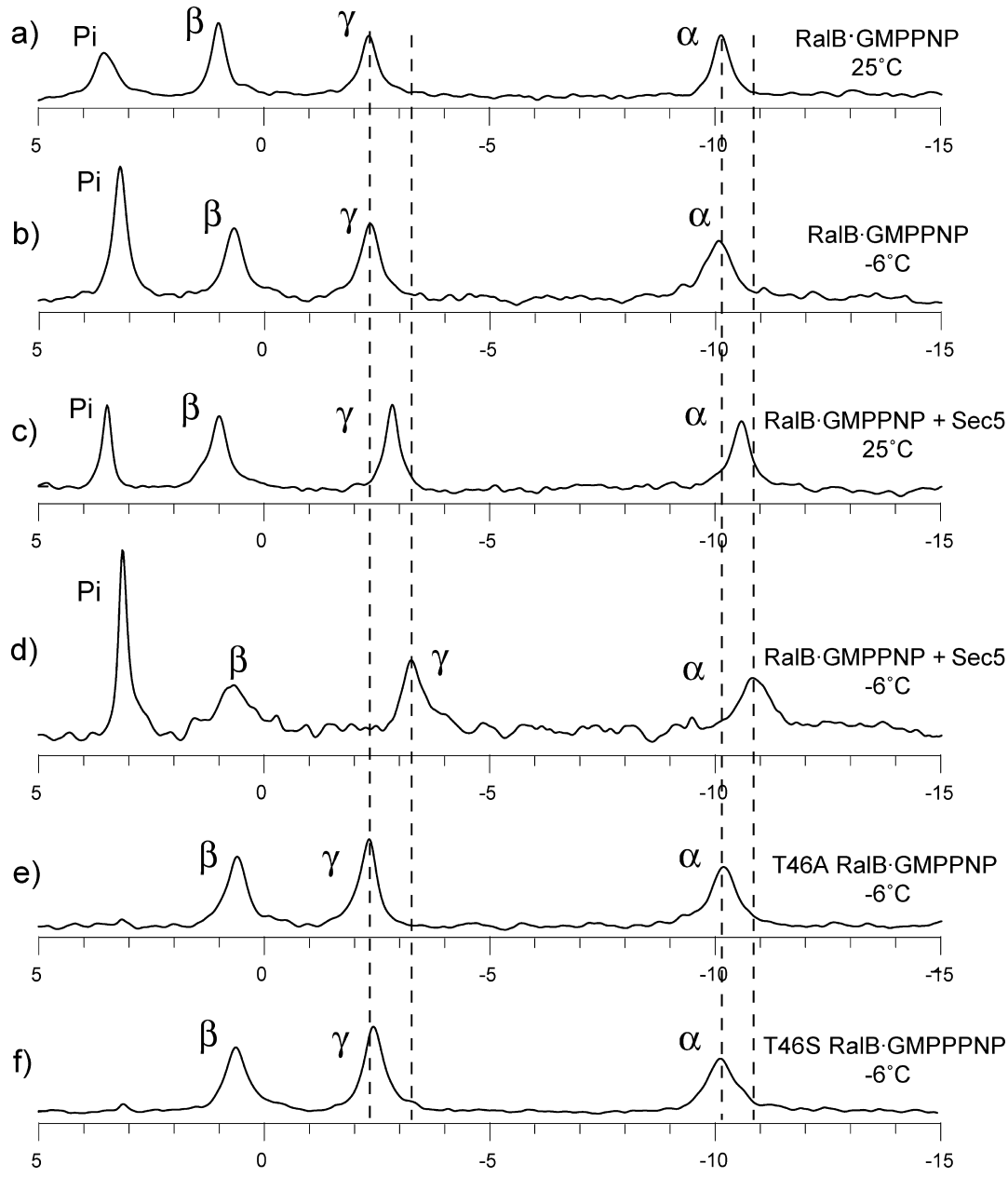

FIGURE 5: ^{31}P NMR spectrum of unlabeled RalB·GMPPNP under different conditions: (a) 25 °C; (b) −6 °C; (c) 25 °C, in the presence of a 2:1 molar excess of the Sec5 GBD; (d) −6 °C, in the presence of a 2:1 molar excess of the Sec5 GBD; (e) the T46A mutant of RalB at −6 °C; (f) the T46S mutant of RalB at −6 °C.

Table 2: Chemical Shifts of Phosphate Resonances at −6 °C

	α-phosphate		*β*-phosphate		*γ*-phosphate	
	1	2	1	2	1	2
RalB·GMPPNP	−10.15		0.67		−2.37	
RalB·GMPPNP + Sec5		−10.91	0.70			−3.30
T46A RalB·GMPPNP	−10.19		0.61		−2.28	
T46S RalB·GMPPNP	−10.12		0.61		−2.44	
RalB·GTP	−9.94	−10.93	−14.20	−14.85	−6.20	−7.52
RalB·GTP + Sec5	−9.96	−11.00	−14.01	−14.36	−6.96	−7.45

resonances in state 2 to be characterized. We thus added excess amounts (2:1) of the Ral effector Sec5. The spectra at 25 and −6 °C both contain a single species (Figure 5c,d), whose α and *γ* chemical shifts are shifted upfield with respect to the uncomplexed RalB (Table 2). The direction of this chemical shift change is consistent with observations on other Ras family proteins that the active, state 2 resonances are shifted upfield with respect to the state 1 resonances (*25*). To confirm that this does indeed correspond to state 2, we used RalB switch I mutants that are designed to stabilize the inactive, state 1 conformation of the G protein. These mutants could be used to determine the chemical shifts of state 1. Work on Ha-Ras has shown that mutation of the invariant Thr35 leads to a protein with a severely reduced affinity for effectors and a ^{31}P NMR spectrum characterized by a single species whose chemicals shifts correspond to state

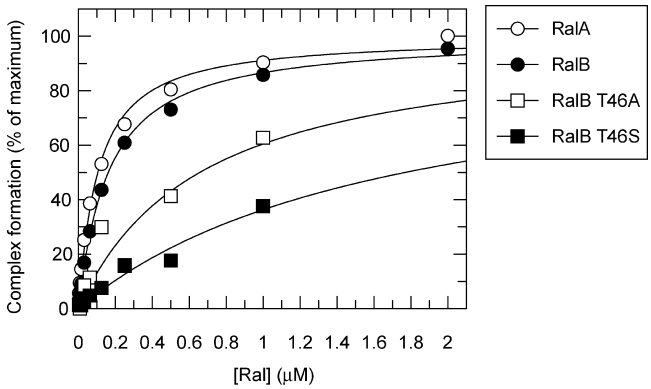

FIGURE 6: Measurement of the affinity of Q72L RalA·GTP, Q72L RalB·GTP, Q72L T46A RalB·GTP, and Q72L T46S RalB·GTP for GST-Sec5 RBD. The indicated concentrations of [^{3}H]GTP-labeled Ral proteins were incubated with 20 nM GST-Sec5 RBD in SPAs. The SPA signal was corrected by subtraction of a blank from which the GST-Sec5 was omitted. The effect of the [G protein] on this corrected SPA counts/min signal was fitted to a binding isotherm to give an apparent K_d value and the signal at saturating concentrations of G protein. The data are expressed as a percentage of this maximum signal. K_d for RalA-Sec5 is 95 ± 10 nM, for RalB-Sec5 is 152 ± 9 nM, for RalB T46A-Sec5 is 648 ± 418 nM, and for RalB T46S-Sec5 is 1650 ± 919 nM.

1 (*60*). We made two mutations at this Thr in RalB, T46S and T46A. The affinities of these mutants for Sec5 were measured using scintillation proximity assays, and their binding was attenuated as expected (Figure 6). In the ^{31}P NMR spectra of both of these mutants (Figure 5e,f) a single resonance is again observed for each phosphate in GMPPNP. As neither mutant is competent to bind to Sec5, these resonances must be at the chemical shifts of the inactive, state 1. Furthermore, the resonances in both mutants are at the same position as those in the spectra of wild-type RalB·GMPPNP in the absence of Sec5 (Table 2, Figure 5). The position of the resonances in the mutant spectra is in agreement with the conclusion that the single species observed for RalB·GMPPNP is indeed in the inactive (state 1) conformation and that the effect of adding Sec5 is to shift the conformation to state 2. The other possibility, that free RalB·GMPPNP is in the active state (state 2) and that in the RalB/Sec5 spectra (Figure 5c,d) the chemical shifts of the phosphate resonances are directly affected by the proximity of Sec5, is less likely, since Sec5 is at least 9 Å away from the nucleotide in the RalA-Sec5 complex (PDB code 1UAD).

We also measured the ^{31}P NMR spectra of RalB bound to its activating nucleotide in cells, GTP. Again, the ^{31}P NMR spectrum at 25 °C contains three resonances (Figure 7a), with chemical shifts of −6.77, −10.48, and −13.82 ppm, which can be assigned to the γ-, α-, and β-phosphate groups, respectively, based on the shifts observed for Ha-Ras·GTP (*25*). At −6 °C, however, each of these resonances splits into two (Figure 7b). The α- and γ-phosphate resonances are split into two resonances of relatively equal size, and comparison of the resonance positions in Figure 7a and Figure 7b indicates that the single resonance at 25 °C is the result of fast exchange between these two components. These two resonances presumably correspond to state 1 and state 2. The β-phosphate resonance at −6 °C is also split into two overlapping components, but in this case the major species is close to the position of the single peak at 25 °C, and a second species, shifted upfield, appears (Table 2). The extra resonances observed at −6 °C are not due to the presence of GDP as a result of GTP hydrolysis during the experiment, since GDP has a distinctive β-phosphate chemical shift of −2 ppm (*61*) and there is no peak at this shift in the spectrum (Figure 7). It is also unlikely that GTP hydrolysis would occur during the time course of the experiments, since the hydrolysis-deficient Q72L mutant of RalB was used in these investigations.

When a molar excess of the Ral effector, Sec5, was added to RalB·GTP, the chemical shifts of the resonances were almost identical to those in the free RalB·GTP spectra at 25 °C (Figure 7c), again indicating that the addition of the effector does not change the chemical environment of the nucleotide. At −6 °C, however, the three phosphate resonances did not coalesce into a single peak corresponding to the active, state 2, suggesting that even in the presence of the effector there was more than one species present (Figure 7d). For the α-phosphate, the two resonances observed are at the same shifts as those in the free RalB at −6 °C, although the peaks are broader. For the β-phosphate and γ-phosphate the two peaks have moved closer together, so that although there are still two discernible resonances they are overlapping.

DISCUSSION

A comparison of RalB·GMPPNP, RalA·GMPPNP (PDB code 1U8Y (*27*)), RalA·GDP (*24*), RalA·GMPPNP in the complexes with Sec5 (1UAD (*28*)) and Exo84 (1ZC3 (*29*)), and RalA·GDP in complex with the *C. botulinum* C3 exoenzyme (C3 Bot) (2A78 (*30*)) shows that the Ral structures are generally similar, with RMSDs across the backbone atoms of 1−2 Å (Table 3, Figure 8). Most differences between the Ral structures are due to the switch regions; RalB·GMPPNP has an RMSD of ∼1 Å when compared to the five RalA structures outside the switches, whereas the RalA structures have pairwise RMSDs of 0.4−0.5 Å when compared to each other. These differences may be genuine divergence between RalA and RalB, but it is more likely that they reflect the fact that all of the RalA structures derive from X-ray crystallographic studies and RalB·GMPPNP is a solution structure.

The RMSDs were calculated with the exclusion of the loop around Ala116, which is the site of an insertion in RalB, since the extra amino acid leads to a significant change in the conformation of this region (Figure 8). The residues in this loop have exceptionally low order parameters, S^2 (Figure 4), and heteronuclear NOE values (Figure 3) indicating a high degree of internal mobility on the picosecond to nanosecond time scale in this region. The temperature factors for this loop were also high in the free and complexed RalA·GMPPNP structures. Taken together, this indicates that there is a high degree of flexibility in the α3−β5 loop in both RalA and RalB. Although it is close, this loop does not directly contact the switch regions and, therefore, the effector binding sites. Analogous regions, also incorporating the C-terminal portion of the neighboring helix α3 in Ras and other small GTPases, have, however, been shown to be part of the binding interface with guanine nucleotide exchange factors (*62, 63*). Aside from the Ala116 insert, Lys120 in RalB is replaced by Asn119 in RalA, which means that this loop in RalB is slightly more basic than that in RalA.

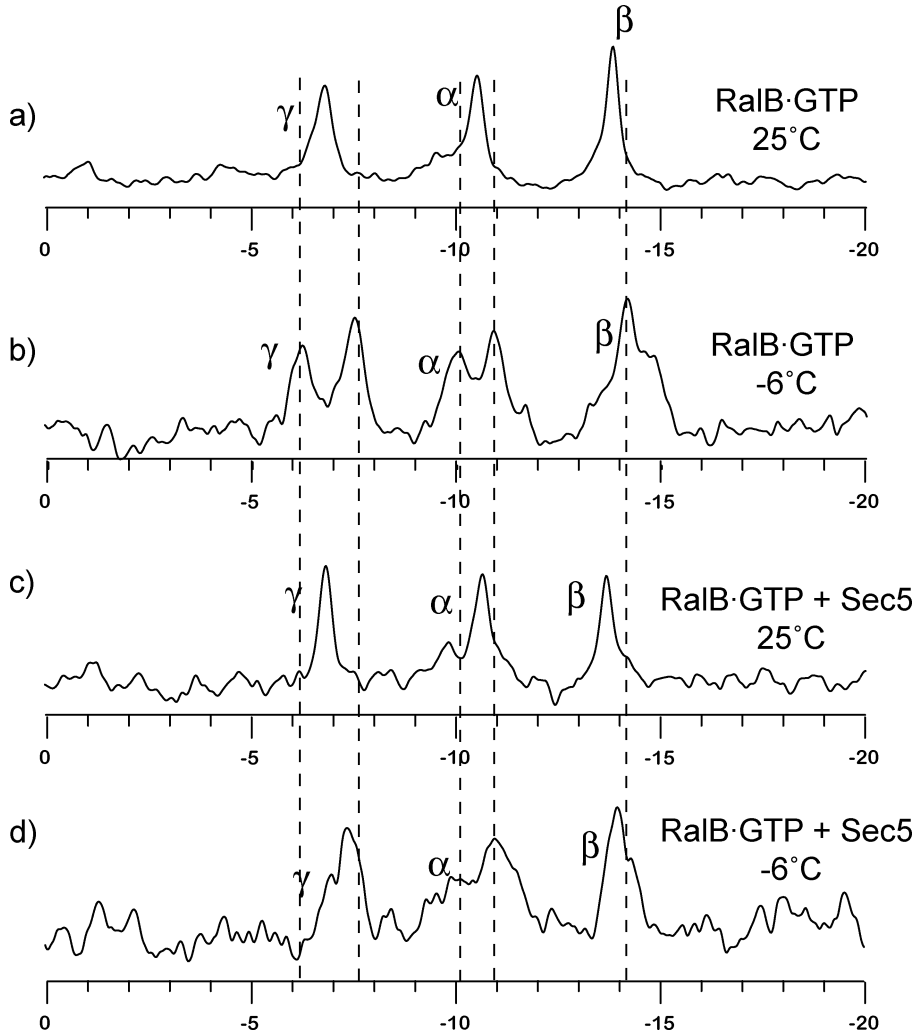

FIGURE 7: ^{31}P NMR spectrum of unlabeled RalB·GTP under four different conditions: (a) 25 °C; (b) −6 °C; (c) 25 °C, in the presence of a 2:1 molar excess of Sec5 GBD; (d) −6 °C, in the presence of a 2:1 molar excess of Sec5 GBD. The K_d of RalB·GTP for the Sec5 GBD is 150 nM (our unpublished results); therefore, the protein concentrations used in this experiment ensure saturation of RalB.

Table 3: Backbone RMSDs of RalB·GMPPNP and RalA Structures (Å)

	RalB·GMPPNP	RalA·GMPPNP	RalA·GMPPNP + Sec5	RalA·GMPPNP + Exo84	RalA·GDP
RalA·GMPPNP (1U8Y chain B)	1.95[a] (1.22)[b]				
RalA·GMPPNP + Sec5 (1UAD) chain B	1.88[a] (1.19)[b]	1.36[d] (0.42)[e]			
RalA·GMPPNP + Exo84 (1ZC3)	1.87[a] (1.11)[b]	1.53[d] (0.55)[e]	0.60[d] (0.36)[e]		
RalA·GDP[c]	1.99[a] (1.13)[b]	1.79[d] (0.47)[e]	1.06[d] (0.41)[e]	0.93[d] (0.44)[e]	
RalA·GDP + exoenzyme C3 (2A78)	2.09[a] (1.15)[b]	1.80[d] (0.47)[e]	1.09[d] (0.42)[e]	0.94[d] (0.45)[e]	0.68[d] (0.36)[e]

[a] Structures were superimposed over residues 13−115, 121−179 (RalB) and 13−115, 120−178 (RalA). [b] Structures were superimposed over residues 13−40, 52−68, 83−115, 121−179 (RalB) and 13−40, 52−68, 83−115, 120−178 (RalA). [c] Coordinates provided by Dr. Ingrid Vetter. [d] Structures were superimposed over residues 13−178. [e] Structures were superimposed over residues 13−40, 52−68, 83−178.

The changes in this loop may provide part of the basis for the different biological roles of RalA and RalB. One study has suggested that residues including this region may be responsible for the differences in binding of exocyst components to RalA and RalB (*8*). RalA was found to coimmunoprecipitate from cell extracts with members of the exocyst complex more strongly than RalB. Investigation of RalA/B and RalB/A chimeras led to the conclusion that residues 91−153 (RalB numbering) play an important role in this differential affinity. This supports the idea that the differences in 116−121 may be responsible for some of the differences between RalA and RalB. The changes in the 116−121 loop would not directly affect the binding of Sec5, which binds exclusively via switch 1 to RalA (*28*) and presumably in a similar manner to RalB (*36*). The differences in this region and in helix 3 could indirectly affect the conformation of the switches. but we have found that the Sec5 RBD interacts with RalA·GTP and RalB·GTP with similar affinities *in vitro* (Figure 6). Our data, however, were generated using GST-Sec5 RBD, while the Shipistin study investigated the interactions of RalA/RalB with Sec5 by coimmunprecipitation. *In vivo*, the presence of full-length Sec5, multiple Ral effectors, including members of the exocyst complex itself, along with the different subcellular localization of RalA and RalB would all influence the observed affinities, unlike those we observe *in vitro*.

To analyze further the dynamics in switch I, we recorded ^{31}P NMR spectra on RalB·GMPPNP (Figure 5). In contrast

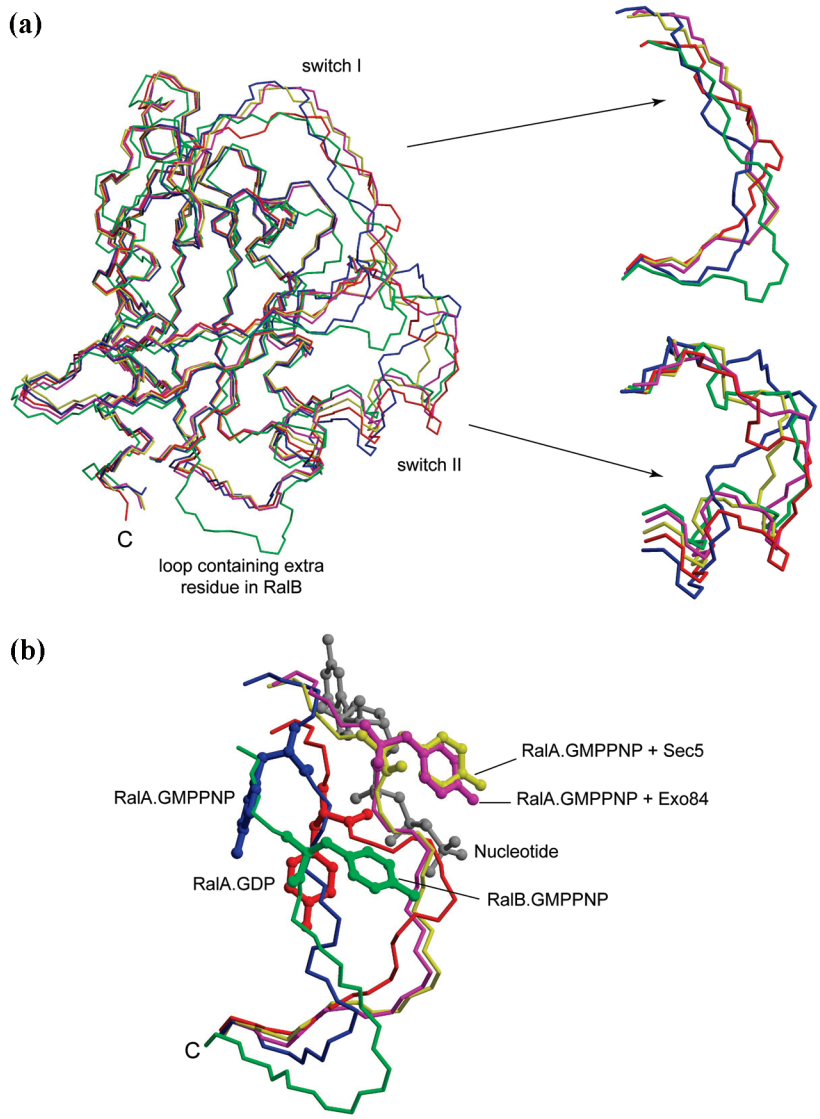

FIGURE 8: Structural alignment of RalB·GMPPNP with various RalA structures. The structures were superimposed over RalB residues 13−115 and 121−178. (a) The backbone traces are shown for each structure: green, RalB·GMPPNP; blue, RalA·GMPPNP; yellow, RalA·GMPPNP from the complex with Sec5; magenta, RalA·GMPPNP from the complex with Exo84; red, RalA·GDP. The panes on the right show the details of the superimposition for switch I (top) and switch II (bottom). (b) The backbone traces for switch I with Tyr43 shown in a ball-and-stick representation. The colors are as in (a), and the different structures are labeled. The position of the nucleotide is shown as a ball-and-stick representation in gray.

to the spectrum of wt Ras·GMPPNP at low temperature (*25*), the three phosphate resonances, although broadened, do not split. There are two explanations for the observation of a single set of resonances in the ^{31}P spectra of RalB·GMPPNP. Perhaps the simplest reason would be that there is indeed only one species in RalB and that the second species is present in such low quantities that it cannot be observed. A second explanation is that there are two species that are exchanging at a rate that is fast on the NMR time scale, and thus a single resonance at the average position of the chemical shifts of the two species is observed. To distinguish between these possibilities, we determined the chemical shifts of the inactive (state 1) and active (state 2) conformations. The chemical shifts of the active conformation were determined by adding an effector protein, in this case Sec5. This led to upfield shifts of ~1 ppm and 0.75 ppm for the α- and γ-phosphate resonances, respectively. The chemical shifts of the inactive conformation were determined using mutations at Thr35 that have been shown to stabilize the inactive, state 1 conformation in Ras (*60*). The equivalent RalB mutants, T46A and T46S, were generated, and the chemical shifts of their phosphate resonances were close to those for the RalB·GMPPNP (Figure 5), suggesting that the latter represent state 1. We can thus conclude that RalB·GMPPNP exists in predominantly one conformation, unlike Ha-Ras·GMPPNP (*25*) and RalA·GMPPNP (*64*). Recent studies of M-Ras·GMPPNP and Cdc42·GMPPNP/GMPPCP suggested that their switches are also in an inactive conformation, and ^{31}P NMR experiments confirmed that state 1 was preferentially populated (*65, 66*).

Evidence from X-ray structures of Cdc42 and M-Ras suggests that state 1 is characterized by a more open structural conformation where there is no interaction between Thr35 (equivalent to Ral Thr46) and the γ-phosphate (*65, 66*). In the RalB·GMPPNP solution structure, the position of the nucleotide and Mg^{2+} was modeled, using the known coordination of the Mg^{2+} ion to Thr28, the β- and γ-phosphates, and two water molecules, thus leaving the sixth coordination

position (usually occupied by Thr46) empty. In contrast to many small G proteins, switch I in RalB·GMPPNP is relatively well defined, and the side chain oxygen of Thr46 is pointing toward the Mg^{2+}. There are unambiguous NOEs from the methyl group of the Thr46 side chain to the Phe82 ring protons and to the Leu67 side chain.

In contrast to Thr46, the side chain of Tyr43 is not well defined and appears to be solvent-exposed, with no long-range NOEs observable. The aromatic side chain of this residue, equivalent to Tyr32 in Ha-Ras, is thought to be responsible for the different ^{31}P shifts observed for the phosphates in state 1 and state 2 of Ha-Ras (*25*), where it was suggested that Tyr32 points toward the β-phosphate in the effector-bound conformation and away from the nucleotide in the inactive state 1. In the RalA-Sec5 effector complex, Tyr43 is indeed pointing toward the β-phosphates (Figure 8b), and ^{31}P NMR shows that it is in state 2 (*64*). In the RalA-Exo84 complex, the Tyr43 side chain is in an almost identical position to that in the Sec5 complex (Figure 8b). In contrast, in the free RalA·GMPPNP structure, the Tyr side chain is pointing away from the nucleotide. It should also be noted that in this structure there are two molecules in the unit cell; in chain A the side chain of Tyr43 is missing whereas in chain B it is in a crystal contact. The position of the side chain is therefore likely to represent just one conformation of the several possible in free RalA·GMPPNP. Tyr43 also points away from the nucleotide in the RalB·GMPPNP solution structure, suggesting that this too is in state 1. The position of the Tyr43 side chain varies among the family of structures calculated from the NMR data, indicating again that multiple conformations are possible.

The NOEs used to calculate the structures of RalB represent the average distances between the nuclei involved during the course of the mixing time. The ^{31}P NMR results and the position of Tyr43 indicate that state 1 is preferentially sampled in solution and thus the NOEs observed would be expected to correspond to those existing in state 1. The ^{15}N relaxation data, along with the lack of backbone resonances for parts of both switch I and II, suggest that both switches are sampling more than one conformation. This suggests that state 1 could represent an ensemble of conformations, as was proposed for Ras (*60, 67*).

In contrast, in the ^{31}P NMR spectrum of RalB·GTP, the resonances are split (Figure 7), in a similar fashion to resonances observed for free Ras·GTP at low temperatures (*25*), and as with Ras, addition of excess effector appears to increase the population of state 2 (*60*). The splitting of RalB·GTP at low temperatures is, however, only diminished and not abolished in the presence of excess Sec5. These experiments were recorded at 0.6 mM RalB·GTP/1.2 mM Sec5, well above the measured K_d for the interaction of 150 nM (Figure 6). This suggests that, even when bound to the effector, the nucleotide is still experiencing more than one environment in the GTP-bound form of the protein. This is markedly different from the situation observed in other G proteins studied by ^{31}P NMR, where binding to an effector protein was shown to uniquely populate state 2.

Thus, free RalB in its GTP-bound form appears to convert between the state 1 and state 2 conformations, even when complexed with downstream effectors. To investigate the effects of this on effector binding, we measured the affinities of both RalA·GTP and RalB·GTP for Sec5 by scintillation proximity assay (SPA). The equilibrium dissociation constant for both Ral proteins for the GBD of Sec5 was very similar; RalA/Sec5 was 95 nM while RalB/Sec5 was 150 nM (Figure 6). These K_ds are similar to that observed for Ha-Ras/Raf complex by the same technique (*68*). For M-Ras, it has been postulated that its preference for state 1 results in low effector affinities (*66*). The K_d obtained with Sec5 indicates that although state 2 is not preferentially stabilized in RalB-effector complexes, the interaction is still of a high affinity, suggesting that both state 1 and state 2 may have a high affinity for effectors. Whether this holds true for all downstream effector proteins of RalB remains to be investigated.

ACKNOWLEDGMENT

We are grateful to Dr. Ingrid Vetter for providing us with the unpublished coordinates for RalA·GDP and to Dr. John Kirkpatrick for helpful discussions.

REFERENCES

1. van Dam, E. M., and Robinson, P. J. (2006) Ral: Mediator of membrane trafficking. *Int. J. Biochem. Cell Biol. 38*, 1841–1847.
2. Rangarajan, A., Hong, S. J., Gifford, A., and Weinberg, R. A. (2004) Species- and cell type-specific requirements for cellular transformation. *Cancer Cell 6*, 171–183.
3. Hamad, N. M., Elconin, J. H., Karnoub, A. E., Bai, W. L., Rich, J. N., Abraham, R. T., Der, C. J., and Counter, C. M. (2002) Distinct requirements for Ras oncogenesis in human versus mouse cells. *Genes Dev. 16*, 2045–2057.
4. Vetter, I. R., and Wittinghofer, A. (2001) Signal transduction—The guanine nucleotide-binding switch in three dimensions. *Science 294*, 1299–1304.
5. Kinsella, B. T., Erdman, R. A., and Maltese, W. A. (1991) Carboxyl-terminal isoprenylation of Ras-related GTP-binding proteins encoded by Rac1, Rac2, and Rala. *J. Biol. Chem. 266*, 9786–9794.
6. Hancock, J. F., Magee, A. I., Childs, J. E., and Marshall, C. J. (1989) All Ras proteins are polyisoprenylated but only some are palmitoylated. *Cell 57*, 1167–1177.
7. Hancock, J. F., Paterson, H., and Marshall, C. J. (1990) A polybasic domain or palmitoylation is required in addition to the CAAX motif to localize p21^{ras} to the plasma membrane. *Cell 63*, 133–139.
8. Shipitsin, M., and Feig, L. A. (2004) RalA but not RalB enhances polarized delivery of membrane proteins to the basolateral surface of epithelial cells. *Mol. Cell. Biol. 24*, 5746–5756.
9. Jilkina, O., and Bhullar, R. P. (1996) Generation of antibodies specific for the RalA and RalB GTP-binding proteins and determination of their concentration and distribution in human platelets. *Biochim. Biophys. Acta 1314*, 157–166.
10. Camonis, J. H., and White, M. A. (2005) Ral GTPases: corrupting the exocyst in cancer cells. *Trends Cell Biol. 15*, 327–332.
11. Jullien-Flores, V., Dorseuil, O., Romero, F., Letourneur, F., Saragosti, S., Berger, R., Tavitian, A., Gacon, G., and Camonis, J. H. (1995) Bridging Ral GTPase to Rho-pathways—Rlip76, a Ral effector with Cdc42/Rac GTPase-activating protein activity. *J. Biol. Chem. 270*, 22473–22477.
12. Cantor, S. B., Urano, T., and Feig, L. A. (1995) Identification and characterization of Ral-binding protein-1, a potential downstream target of Ral GTPases. *Mol. Cell. Biol. 15*, 4578.
13. Park, S. H., and Weinberg, R. A. (1995) A putative effector of Ral has homology to Rho/Rac GTPase activating proteins. *Oncogene 11*, 2349.
14. Jullien-Flores, V., Mahe, Y., Mirey, G., Leprince, C., Meunier-Bisceuil, B., Sorkin, A., and Camonis, J. H. (2000) RLIP76, an effector of the GTPase Ral, interacts with the AP2 complex: involvement of the Ral pathway in receptor endocytosis. *J. Cell Sci. 113*, 2837–2844.
15. Yamaguchi, A., Urano, T., Goi, T., and Feig, L. A. (1997) An eps homology (EH) domain protein that binds to the Ral-GTPase target, RalBP1. *J. Biol. Chem. 272*, 31230.
16. Frankel, P., Aronheim, A., Kavanagh, E., Balda, M. S., Matter, K., Bunney, T. D., and Marshall, C. J. (2005) RalA interacts with

ZONAB in a cell density-dependent manner and regulates its transcriptional activity. *EMBO J. 24*, 54.
17. Sidhu, R. S., Clough, R. R., and Bhullar, R. P. (2005) Regulation of phospholipase C-d1 through direct interactions with the small GTPase Ral and calmodulin. *J. Biol. Chem. 280*, 21933.
18. Jiang, H., Luo, J. Q., Urano, T., Frankel, P., Lu, Z. M., Foster, D. A., and Feig, L. A. (1995) Involvement of Ral GTPase in V-Src-induced phospholipase-D activation. *Nature 378*, 409.
19. Ohta, Y., Suzuki, N., Nakamura, S., Hartwig, J. H., and Stossel, T. P. (1999) The small GTPase RalA targets filamin to induce filopodia. *Proc. Natl. Acad. Sci. U.S.A. 96*, 2122–2128.
20. Chien, Y. C., and White, M. A. (2003) RAL GTPases are linchpin modulators of human tumour-cell proliferation and survival. *EMBO Rep. 4*, 800.
21. Lim, K. H., Baines, A. T., Fiordalisi, J. J., Shipitsin, M., Feig, L. A., Cox, A. D., Der, C. J., and Counter, C. M. (2005) Activation of RaIA is critical for Ras-induced tumorigenesis of human cells. *Cancer Cell 7*, 533.
22. Rosse, C., Hatzoglou, A., Parrini, M. C., White, M. A., Chavrier, P., and Camonis, J. (2006) RalB mobilizes the exocyst to drive cell migration. *Mol. Cell. Biol. 26*, 727.
23. Chien, Y. C., Kim, S., Bumeister, R., Loo, Y. M., Kwon, S. W., Johnson, C. L., Balakireva, M. G., Romeo, Y., Kopelovich, L., Gale, M., Yeaman, C., Camonis, J. H., Zhao, Y. M., and White, M. A. (2006) RaIB GTPase-mediated activation of the I kappa B family kinase TBK1 couples innate immune signaling to tumor cell survival. *Cell 127*, 157–170.
24. Bauer, B., Mirey, G., Vetter, I. R., Garcia-Ranea, J. A., Valencia, A., Wittinghofer, A., Camonis, J. H., and Cool, R. H. (1999) Effector recognition by the small GTP-binding proteins Ras and Ral. *J. Biol. Chem. 274*, 17763–17770.
25. Geyer, M., Schweins, T., Herrmann, C., Prisner, T., Wittinghofer, A., and Kalbitzer, H. R. (1996) Conformational transitions in p21(ras) and in its complexes with the effector protein Raf-RBD and the GTPase activating protein GAP. *Biochemistry 35*, 10308–10320.
26. Ito, Y., Yamasaki, K., Iwahara, J., Terada, T., Kamiya, A., Shirouzu, M., Muto, Y., Kawai, G., Yokoyama, S., Laue, E. D., Walchli, M., Shibata, T., Nishimura, S., and Miyazawa, T. (1997) Regional polysterism in the GTP-bound form of the human c-Ha-Ras protein. *Biochemistry 36*, 9109–9119.
27. Nicely, N. I., Kosak, J., de Serrano, V., and Mattos, C. (2004) Crystal structures of Ral-GppNHp and Ral-GDP reveal two binding sites that are also present in Ras and Rap. *Structure 12*, 2025–2036.
28. Fukai, S., Matern, H. T., Jagath, J. R., Scheller, R. H., and Brunger, A. T. (2003) Structural basis of the interaction between RalA and Sec5, a subunit of the sec6/8 complex. *EMBO J. 22*, 3267.
29. Jin, R. S., Junutula, J. R., Matern, H. T., Ervin, K. E., Scheller, R. H., and Brunger, A. T. (2005) Exo84 and Sec5 are competitive regulatory Sec6/8 effectors to the RalA GTPase. *EMBO J. 24*, 2064.
30. Pautsch, A., Vogelsgesang, M., Trankle, J., Herrmann, C., and Aktories, K. (2005) Crystal structure of the C3bot-RalA complex reveals a novel type of action of a bacterial exoenzyme. *EMBO J. 24*, 3670–3680.
31. Holbourn, K. P., Sutton, J. M., Evans, H. R., Shone, C. C., and Acharya, K. R. (2005) Molecular recognition of an ADP-ribosylating *Clostridium botulinum* C3 exoenzyme by RaIA GTPase. *Proc. Natl. Acad. Sci. U.S.A. 102*, 5357–5362.
32. Mott, H. R., Owen, D., Nietlispach, D., Lowe, P. N., Manser, E., Lim, L., and Laue, E. D. (1999) Structure of the small G protein Cdc42 bound to the GTPase- binding domain of ACK. *Nature 399*, 384–388.
33. Morreale, A., Venkatesan, M., Mott, H. R., Owen, D., Nietlispach, D., Lowe, P. N., and Laue, E. D. (2000) Structure of Cdc42 bound to the GTPase binding domain of PAK. *Nat. Struct. Biol. 7*, 384–388.
34. Prasannan, S., Fenwick, R. B., Campbell, L. J., Evetts, K. A., Nietlispach, D., Owen, D., and Mott, H. R. (2007) ^{1}H, ^{13}C and ^{15}N resonance assignments for the small G protein RalB in its active conformation. *Biomol. NMR Assign. 1*, 147–149.
35. Thompson, G., Owen, D., Chalk, P. A., and Lowe, P. N. (1998) Delineation of the Cdc42/Rac-binding domain of p21-activated kinase. *Biochemistry 37*, 7885–7891.
36. Mott, H. R., Nietlispach, D., Hopkins, L. J., Mirey, G., Camonis, J. H., and Owen, D. (2003) Structure of the GTPase-binding domain of Sec5 and elucidation of its Ral binding site. *J. Biol. Chem. 278*, 17053–17059.
37. Graham, D. L., Eccleston, J. F., Chung, C. W., and Lowe, P. N. (1999) Magnesium fluoride-dependent binding of small G proteins to their GTPase-activating proteins. *Biochemistry 38*, 14981–14987.
38. Skinner, R. H., Picardo, M., Gane, N. M., Cook, N. D., Morgan, L., Rowedder, J., and Lowe, P. N. (1994) Direct measurement of the binding of Ras to neurofibromin using a scintillation proximity assay. *Anal. Biochem. 223*, 259–265.
39. Owen, D., Campbell, L. J., Littlefield, K., Evetts, K. A., Li, Z. G., Sacks, D. B., Lowe, P. N., and Mott, H. R. (2008) The IQGAP1-Rac1 and IQGAP1-Cdc42 interactions—Interfaces differ between the complexes. *J. Biol. Chem. 283*, 1692–1704.
40. Owen, D., Lowe, P. N., Nietlispach, D., Brosnan, C. E., Chirgadze, D. Y., Parker, P. J., Blundell, T. L., and Mott, H. R. (2003) Molecular dissection of the interaction between the small G proteins Rac1 and RhoA and protein kinase C-related kinase 1 (PRK1). *J. Biol. Chem. 278*, 50578–50587.
41. Owen, D., Mott, H. R., Laue, E. D., and Lowe, P. N. (2000) Residues in Cdc42 that specify binding to individual CRIB effector proteins. *Biochemistry 39*, 1243–1250.
42. Graham, D. L., Eccleston, J. F., and Lowe, P. N. (1999) The conserved arginine in Rho-GTPase-activating protein is essential for efficient catalysis but not for complex formation with rho CDP and aluminum fluoride. *Biochemistry 38*, 985–991.
43. Vranken, W. F., Boucher, W., Stevens, T. J., Fogh, R. H., Pajon, A., Llinas, P., Ulrich, E. L., Markley, J. L., Ionides, J., and Laue, E. D. (2005) The CCPN data model for NMR spectroscopy: Development of a software pipeline. *Proteins: Struct., Funct., Bioinf. 59*, 687–696.
44. Farrow, N. A., Zhang, O. W., Formankay, J. D., and Kay, L. E. (1994) A heteronuclear correlation experiment for simultaneous determination of N-15 longitudinal decay and chemical-exchange rates of systems in slow equilibrium. *J. Biomol. NMR 4*, 727–734.
45. Efron, B., and Tibshirani, F. (1986) Bootstrap methods for standard errors, confidence intervals and other measures of statistical accuracy. *Stat. Sci. 1*, 54–77.
46. Dosset, P., Hus, J. C., Blackledge, M., and Marion, D. (2000) Efficient analysis of macromolecular rotational diffusion from heteronuclear relaxation data. *J. Biomol. NMR 16*, 23–28.
47. de Alba, E., Baber, J. L., and Tjandra, N. (1999) The use of residual dipolar coupling in concert with backbone relaxation rates to identify conformational exchange by NMR. *J. Am. Chem. Soc. 121*, 4282–4283.
48. Barbato, G., Ikura, M., Kay, L. E., Pastor, R. W., and Bax, A. (1992) Backbone dynamics of calmodulin studied by N-15 relaxation using inverse detected 2-dimensional NMR spectroscopy—The central helix is flexible. *Biochemistry 31*, 5269–5278.
49. Lipari, G., and Szabo, A. (1982) Model-free approach to the interpretation of nuclear magnetic-resonance relaxation in macromolecules. 1. Theory and range of validity. *J. Am. Chem. Soc. 104*, 4546–4559.
50. Lipari, G., and Szabo, A. (1982) Model-free approach to the interpretation of nuclear magnetic-resonance relaxation in macromolecules. 2. Analysis of experimental results. *J. Am. Chem. Soc. 104*, 4559–4570.
51. Clore, G. M., Szabo, A., Bax, A., Kay, L. E., Driscoll, P. C., and Gronenborn, A. M. (1990) Deviations from the simple 2-parameter model-free approach to the interpretation of N-15 nuclear magnetic-relaxation of proteins. *J. Am. Chem. Soc. 112*, 4989–4991.
52. Mandel, A. M., Akke, M., and Palmer, A. G. (1995) Backbone dynamics of *Escherichia-coli* ribonuclease Hi—Correlations with structure and function in an active enzyme. *J. Mol. Biol. 246*, 144–163.
53. Cornilescu, G., Delaglio, F., and Bax, A. (1999) Protein backbone angle restraints from searching a database for chemical shift and sequence homology. *J. Biomol. NMR 13*, 289–302.
54. Linge, J. P., O'Donoghue, S. I., and Nilges, M. (2001) Automated assignment of ambiguous NOEs with ARIA. *Methods Enzymol. 339*, 71–90.
55. Brunger, A. T., Adams, P. D., Clore, G. M., DeLano, W. L., Gros, P., Grosse-Kunstleve, R. W., Jiang, J. S., Kuszewski, J., Nilges, M., Pannu, N. S., Read, R. J., Rice, L. M., Simonson, T., and Warren, G. L. (1998) Crystallography & NMR system: A new software suite for macromolecular structure determination. *Acta Crystallogr., Sect. D: Biol. Crystallogr. 54*, 905–921.
56. Gardner, K. H., and Kay, L. E. (1998) The use of H-2, C-13, N-15 multidimensional NMR to study the structure and dynamics of proteins. *Annu. Rev. Biophys. Biomol. Struct. 27*, 357–406.
57. Feltham, J. L., Dotsch, V., Raza, S., Manor, D., Cerione, R. A., Sutcliffe, M. J., Wagner, G., and Oswald, R. E. (1997) Definition

of the switch surface in the solution structure of Cdc42Hs. *Biochemistry 36*, 8755–8766.
58. Wuthrich, K. (1986) *NMR of Proteins and Nucleic Acids*, Wiley Interscience, New York.
59. Iuga, A., Spoerner, M., Kalbitzer, H. R., and Brunner, E. (2004) Solid-state P-31 NMR spectroscopy of microcrystals of the Ras protein and its effector loop mutants: Comparison between crystalline and solution state. *J. Mol. Biol. 342*, 1033–1040.
60. Spoerner, M., Herrmann, C., Vetter, I. R., Kalbitzer, H. R., and Wittinghofer, A. (2001) Dynamic properties of the Ras switch I region and its importance for binding to effectors. *Proc. Natl. Acad. Sci. U.S.A. 98*, 4944–4949.
61. Rosch, P., Wittinghofer, A., Tucker, J., Sczakiel, G., Leberman, R., and Schlichting, I. (1986) P-31-NMR spectra of the Ha-Ras p21 nucleotide complexes. *Biochem. Biophys. Res. Commun. 135*, 549–555.
62. Boriack-Sjodin, P. A., Margarit, S. M., Bar-Sagi, D., and Kuriyan, J. (1998) The structural basis of the activation of Ras by Sos. *Nature 394*, 337–343.
63. Day, G. J., Mosteller, R. D., and Broek, D. (1998) Distinct subclasses of small GTPases interact with guanine nucleotide exchange factors in a similar manner. *Mol. Cell. Biol. 18*, 7444–7454.
64. Liao, J. L., Shima, F., Araki, M., Ye, M., Muraoka, S., Sugimoto, T., Kawamura, M., Yamamoto, N., Tamura, A., and Kataoka, T. (2008) Two conformational states of Ras GTPase exhibit differential GTP-binding kinetics. *Biochem. Biophys. Res. Commun. 369*, 327–332.
65. Phillips, M. J., Calero, G., Chan, B., Ramachandran, S., and Cerione, R. A. (2008) Effector proteins exert an important influence on the signaling-active state of the small GTPase Cdc42. *J. Biol. Chem. 283*, 14153–14164.
66. Ye, M., Shima, F., Muraoka, S., Liao, J. L., Okamoto, H., Yamamoto, M., Tamura, A., Yagi, N., Ueki, T., and Kataoka, T. (2005) Crystal structure of M-Ras reveals a GTP-bound "off" state conformation of Ras family small GTPases. *J. Biol. Chem. 280*, 31267–31275.
67. Spoerner, M., Wittinghofer, A., and Kalbitzer, H. R. (2004) Perturbation of the conformational equilibria in Ras by selective mutations as studied by P-31 NMR spectroscopy. *FEBS Lett. 578*, 305–310.
68. Gorman, C., Skinner, R. H., Skelly, J. V., Neidle, S., and Lowe, P. N. (1996) Equilibrium and kinetic measurements reveal rapidly reversible binding of ras to raf. *J. Biol. Chem. 271*, 6713–6719.
69. Laskowski, R. A., Macarthur, M. W., Moss, D. S., and Thornton, J. M. (1993) Procheck—A program to check the stereochemical quality of protein structures. *J. Appl. Crystallogr. 26*, 283–291.
70. Kraulis, P. J. (1991) Molscript—A program to produce both detailed and schematic plots of protein structures. *J. Appl. Crystallogr. 24*, 946–950.
71. Merritt, E. A., and Bacon, D. J. (1997) Raster3D: Photorealistic molecular graphics, in *Macromolecular Crystallography*, Part B, pp 505—524, Elsevier, San Diego, CA.

BI802129D